Macromolecules

Volume 30, Number 15 July 28, 1997

Phase Behavior and Molecular Structure of Liquid-Crystalline Polyesters with Flexible Lateral Substituents

Pio Iannelli*

Dipartimento di Ingegneria Chimica ed Alimentare, Universitá di Salerno, via Ponte Don Melillo, I-84084 Fisciano (Salerno), Italy

Stefania Pragliola, Antonio Roviello, and Augusto Sirigu

Dipartimento di Chimica, Universitá "Federico II" di Napoli, via Mezzocannone 4, I-80134 Napoli, Italy

Received October 15, 1996; Revised Manuscript Received May 13, 1997[⊗]

ABSTRACT: The characterization of segmented liquid-crystalline polyesters (LCP's) with short flexible lateral substituents is reported. The general formula of polymers is $[-p\text{-}C_6H_4OOC\text{-}p\text{-}C_6H_3(R)COO\text{-}p\text{-}C_6H_4O(CH_2)_nO-]_x$, with $n = 2$ and $R = -O(CH_2)_{m-1}CH_3$ ($m = 1-4$). They have nematic liquid-crystalline behavior. At room temperature, polymers show a crystalline phase, whose structure has been solved for the term with $n = 3$. Cell parameters are $a = 13.20(1)$ Å, $b = 6.48(1)$ Å, $c = 20.11(2)$ Å, $\alpha = 138.3(1)°$, $\beta = 110.9(1)°$, and $\gamma = 80.8(1)°$ (space group $P\bar{1}$, two chains per cell, $\rho_c = 1.367$ g cm^{-3}). The molecular packing is characterized by the organization of chains in double stacks with the lateral flexible substituents confined in between.

Introduction

Main-chain liquid-crystalline polyesters (LCP's), with both semiflexible (*segmented* LCP) and linear rigid chains (*rodlike* LCP), have been largely investigated mostly in connection with the manufacture of materials with enhanced mechanical properties. In the case of rodlike LCP, the stiffness of the macromolecular chain raises melting and softening temperatures to such a level that processability of the material becomes difficult. It has been shown that the insertion of flexible groups as side pendants of the macromolecular chain may be a practicable way to lower the melting temperature,[1−7] giving liquid crystallinity and, consequently, improving bulk processability and/or solubility in organic solvents.[8,9] As the insertion of a flexible segment along the main chain has a similar role, the joint presence of this feature and of flexible side-chain substituents may allow one to modulate relevant properties of a mesogenic polymer within a large range of values. On the other side, it has been found that long side chain substituents may have a deep influence not only on the solid state structure but also on the nature of the liquid crystalline phase producing peculiar layered (sanidic) structures.[1] We have recently reported on the phase properties of the following set of polymers, namely **P**(*m*,*n*).[10]

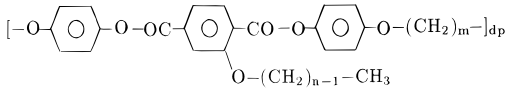

P(m, n) m = 2, 4 n = 5, 6, 7, 8

For these polymers, even with $m = 2$, both T_m and T_i are considerably lowered ($150 \leq T_m \leq 190$ °C; $210 \leq T_i \leq 235$ °C) and the liquid crystalline behavior is perfectly enantiotropic. It has also been shown that as extruded fibers may exhibit at room temperature a further mesomorphic structure which eventually crystallizes by annealing. In order to complete the study of the phase behavior of polymers **P**(2,*n*) exploring the small-*n* side of the homologous series, with the aim of possibly obtaining the most simple polymer for a detailed structural analysis whose thermal and structural behavior could be taken as a fair representative for the all series, polymers **P**(2,*n*) with $n = 1,4$ were synthesized and their phase behavior examined. Polymer **P**(2,3) was selected for performing a complete X-ray diffraction analysis.

Experimental Section

Polymers **P**(2,*n*) were synthesized following the procedure outlined in ref 10. For all polymers synthesized the ^{1}H NMR data, obtained by means of a Varian XL 200 MHz apparatus, are consistent with the formula. Proton resonance data at 50

[⊗] Abstract published in *Advance ACS Abstracts,* July 1, 1997.

S0024-9297(96)01523-9 CCC: $14.00

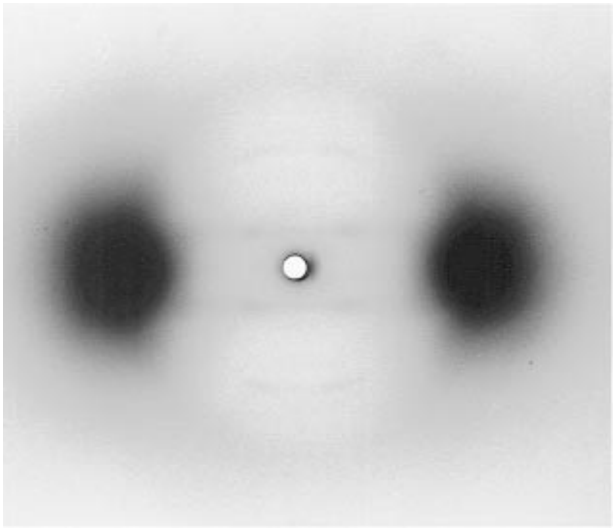

Figure 1. X-ray diffraction pattern at room temperature of a fiber sample of **P**(2,1) as obtained from the extrusion.

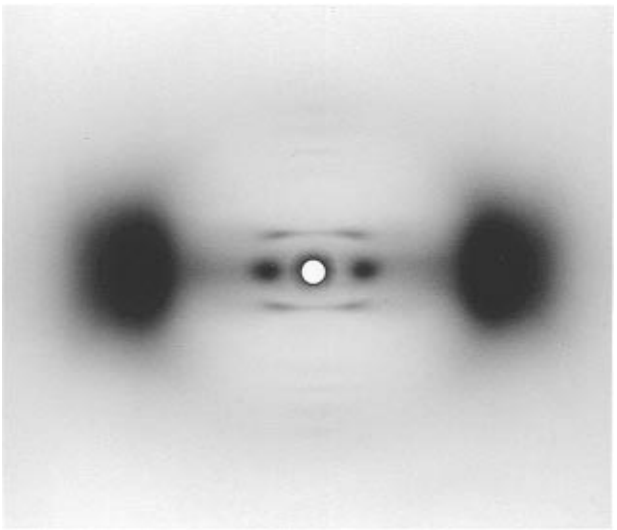

Figure 2. X-ray diffraction pattern at room temperature of a fiber sample of **P**(2,4) as obtained from the extrusion.

C° (1,1,2,2-tetrachloroethane-d_2 as solvent) are specifically reported for polymer **P**(2,4) as an example:

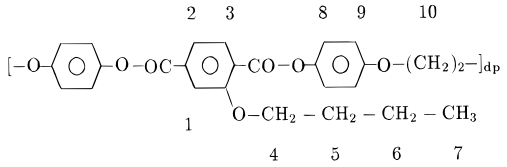

^{1}H NMR, position (δ (ppm)): 1,2 (7.8); 3 (8.1); 4 (4.2); 5 (1.9); 6 (1.6); 7 (1.0); 8 (7.2); 9 (7.1); 10 (4.4). Fiber samples of **P**(2,*n*) were extruded from the anisotropic liquid phase and cooled in the air without temperature control. Thermal treatments were carried out on fiber samples by means of a DSC-7 Perkin-Elmer calorimeter under nitrogen flow at a 10 °C/min rate. Optical microscopy was performed by using a Jenapol microscope fitted with a Linkam THMS 600 hot stage. Fiber diffraction spectra were recorded under vacuum by means of a cylindrical camera with a radius of 57.3 mm. Cr Kα radiation, monochromatized by a flat graphite single crystal, was employed to ensure a better spectral resolution. The high-temperature X-ray diffraction patterns (200 °C, Cu Kα Ni-filtered radiation) were collected using a flat camera and a microfurnace. The diffraction pattern used for the structural refinement were digitized (128 dpi) by means of a Deskscan HP-II CX scanner equipped with a transparencies adaptor.[11] To avoid saturation problem, two films with different exposure times (60 and 10 min) were merged into a single pattern. The preliminary data processing for obtaining diffraction intensity data from the optical density measurements followed the procedure outlined in ref 12. The background intensity due to incoherent scattering and to amorphous material was not subtracted *ab initio* and it was considered in the fitting stage.

Characterization of Phase Behavior

Polymers **P**(2,*n*) are thermotropic. They melt to the nematic phase according to the X-ray diffraction and optical observations at high temperature. The X-ray diffraction patterns recorded at 200 °C are characterized by a partially polarized equatorial halo peaked at about $(\sin\theta)/\lambda = 0.11$ Å^{-1}. No Bragg diffraction is observed for lattice distances lower than ≈40 Å. The X-ray diffraction patterns recorded at room temperature indicate for all polymers a mesomorphic structure. This is close to a supercooled (cybotactic) nematic for **P**(2,1) and **P**(2,2) (Figure 1) and more strictly structured for **P**(2,3) and **P**(2,4) as detectable by the presence of a sharp equatorial diffraction at $d = 15.6$ Å (Figure 2). The same mesophase was found in the case of **P**(2,*n*) with $n > 4$.[10]

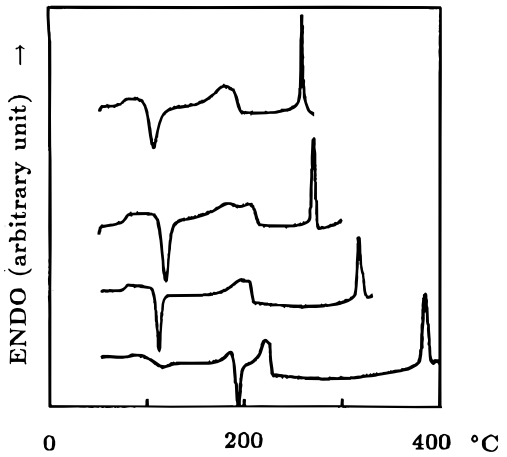

Figure 3. DSC heating traces of fiber samples of **P**(2,*n*). From bottom to top: **P**(2,1), **P**(2,2), **P**(2,3), and **P**(2,4).

Table 1. Thermodynamic Data[a]

polymer	T_m (°C)	ΔH_m (J g^{-1})	T_i (°C)	ΔH_i (J g^{-1})	T_g[b] (°C)	ρ[c] (g cm^{-3})	$[\eta]$[d] (dL g^{-1})
P(2,1)	223	27.8	384	22.5	83	1.22	1.35
P(2,2)	200	29.6	317	15.4	79	1.28	1.11
P(2,3)	195	32.7	272	12.5	82	1.28	2.20
P(2,4)	188	27.3	259	10.0	72	1.20	1.80

[a] T_m = melting temperature; ΔH_m = melting enthalpy; T_g = glassy temperature. Data are referred to fiber samples of polymers annealed 3 h at a temperature 10 °C less than T_m. [b] Glassy temperatures were evaluated by analyzing the DSC heating traces. [c] Density of as extruded fiber samples measured at 25.0 °C by flotation [$\sigma(\rho)/\rho = 0.005$]. [d] Intrinsic viscosity evaluated in 1,1,2,2-tetrachloroethane at 55.0 °C.

DSC analysis was performed on fiber samples. The first heating scans are compared in Figure 3. Thermodynamic data are given in Table 1. The exothermic transition at about 120 °C, which appears in all traces, corresponds to the crystallization to a phase, namely phase I, the structure analysis of which will be reported below for **P**(2,3). The X-ray diffraction pattern of phase I is shown in Figure 4 for **P**(2,1). At higher temperatures, the two endothermic transitions correspond to the melting to the nematic phase and to the isotropization, respectively. Actually, the melting peak is the overlap

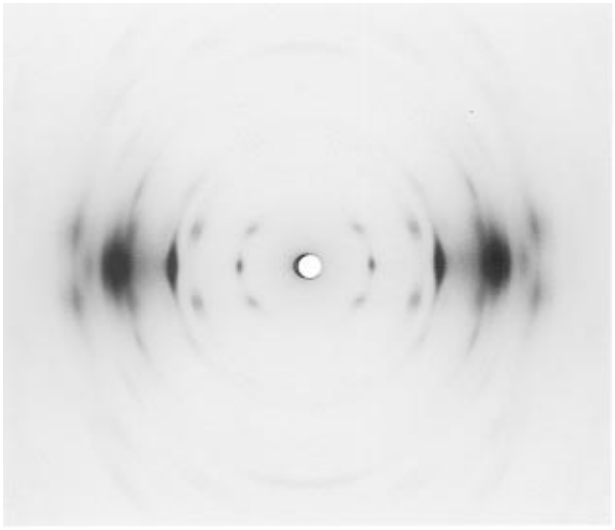

Figure 4. X-ray diffraction pattern at room temperature of a fiber sample of **P**(2,1) heated up to 150 °C and cooled down to room temperature (phase I).

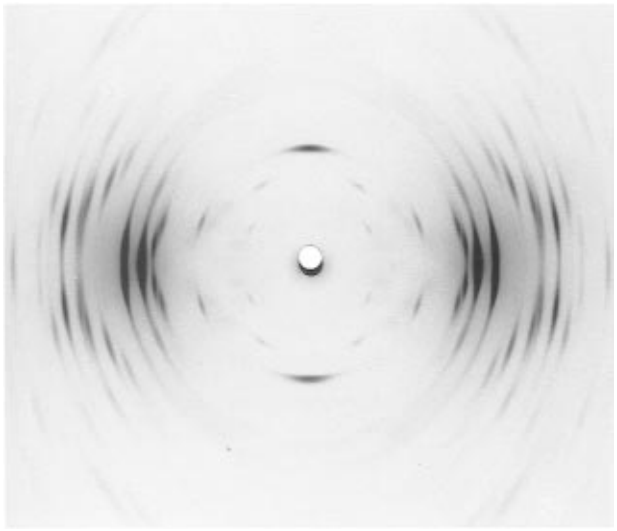

Figure 5. X-ray diffraction pattern at room temperature of a fiber sample of **P**(2,1) heated up to 210 °C and cooled down to room temperature (phase II).

of at least two endothermic peaks which may be connected to a premelt recrystallization phenomena or to a solid-to-solid transition. In this study, no evidence in favor of polymorphic behavior was found, excepted for **P**(2,1) (see below). Isotropization temperatures decrease by increasing the length of flexible lateral insertion, following a strongly nonlinear trend. It is noteworthy that T_i[**P**(2,4)] is about 25 °C higher than T_i[**P**(2,5)] while only 10 °C separates the latter from T_i[**P**(2,8)].[10]

P(2,1) shows one more exothermic transition at about 190 °C which accompanies the appearing of one more crystalline phase, namely phase II (Figure 5). The transition from phase I to phase II is not reversible (see Figure 6). Phase I is obtained only from the mesomorphic form by annealing at temperatures higher than 115 °C. However, although the formation of phase II is very fast at temperature ≥190 °C, the rate is appreciable also at lower temperature. Actually, while a mesomorphic sample heated at 150 °C shows a nearly complete transformation to phase I, its annealing at 180 °C produces both phase I and phase II (Figure 7).

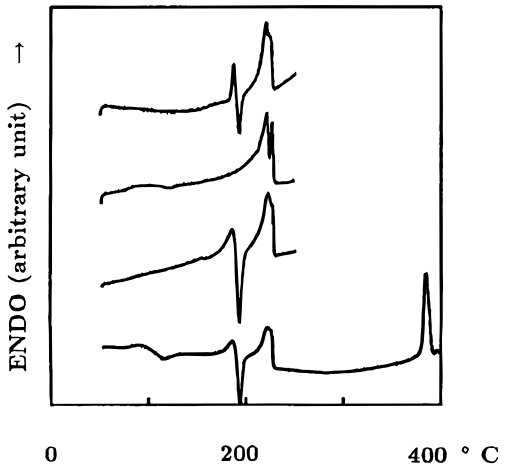

Figure 6. DSC heating traces of fiber samples of **P**(2,1). From bottom to top: sample as extruded; sample previously heated at 150 °C (phase I); sample previously heated at 210 °C (phase II); sample previously annealed for 3 h at 180 °C (phase I + phase II).

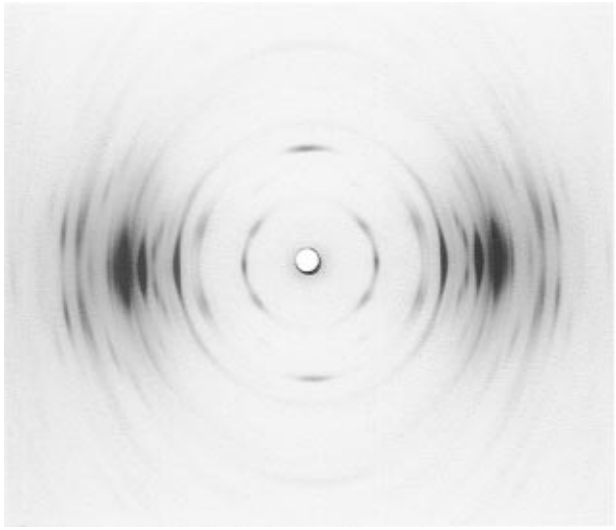

Figure 7. X-ray diffraction pattern at room temperature of a fiber sample of **P**(2,1) annealed for 3 h at 180 °C (phase I + phase II).

Molecular Structure Analysis of P(2,3)

Initial Analysis. The Bragg reflections in the X-ray diffraction pattern of fiber samples of **P**(2,*n*), with the exception of **P**(2,1), are not perfectly aligned along the layer lines, *i.e.* the lines at constant value of Bragg index *l* (see Figure 8). Thus, the axis of preferential orientation of crystallites is tilted with respect to the fiber axis direction. The tilting can be quantified in the reciprocal space by the angle μ, *i.e.* the angle of rotation of crystallites around the vector $\vec{\rho}_t$. The direction of $\vec{\rho}_t$ is conveniently defined by the two angles ω_t and σ_t[13] (see Figure 9). In the case of **P**(2,*n*), $\vec{\rho}_t$ is quite parallel to the direction of the reciprocal lattice axis *a**.

A preliminary comparison of the X-ray diffraction patterns suggests that the crystal structures of all polymers in phase I are substantially isomorphic. The choice to carry out the complete crystal analysis of **P**(2,3) was based on the better quality of the diffraction pattern and on the expectation of having a more significant picture of the sterical role of the lateral substituents. The diffraction pattern of **P**(2,3) is roughly accounted for by the triclinic cell with the following lattice constants: a = 13.1 Å, b = 6.4 Å, c = 20.8 Å, α

Table 2. Cell Parameters of Phase I[a]

polymer	*a* (Å)	*b* (Å)	*c* (Å)	α (deg)	*β* (deg)	*γ* (deg)	*μ* (deg)	ρ_c (g cm^{-3})
P(2,1)	14.03(4)	6.43(15)	20.1(4)	134.7(1.8)	117.8(2.5)	84.9(2.2)	0	1.217
P(2,2)	13.22(5)	6.73(4)	20.1(1)	140.0(3)	111.4(6)	82.0(5)	1.30(9)	1.284
P(2,3)	13.20(1)	6.48(1)	20.11(2)	138.3(1)	110.9(1)	80.8(1)	3.25(1)	1.367
P(2,4)	13.36(5)	6.67(5)	20.1(2)	139.8(4)	106.1(8)	86.5(7)	3.9(1)	1.349

[a] Cell parameters were evaluated by best fit of the eight strongest X-ray diffraction spots. Standard deviations are given in parentheses. The cell parameters of **P**(2,3), refined by means of the whole-pattern method, are given for a comparison.

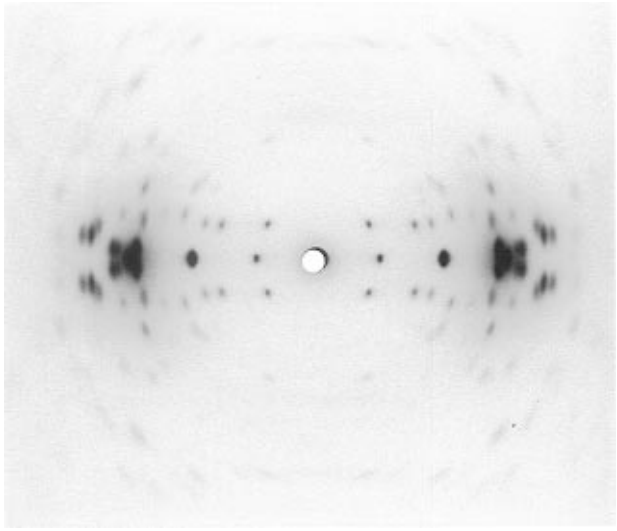

Figure 8. X-ray diffraction pattern at room temperature of a fiber sample of **P**(2,3) annealed for 3 h at 185 °C.

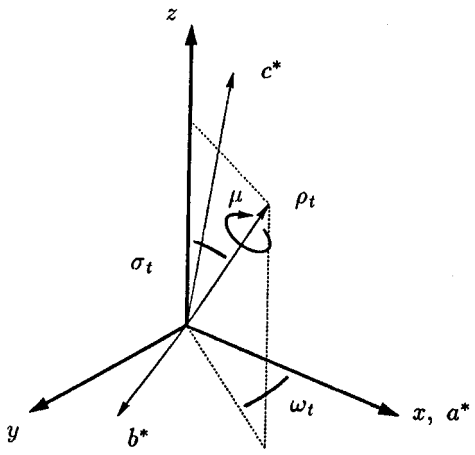

Figure 9. Geometrical parameters relative to crystallites tilting.

= 140°, β = 114°, and γ = 77° (two chain per unit cell). A reliable starting value for the tilting angle is $\mu \approx 2°$. These values were obtained by the best fit of the eight strongest X-ray diffraction spots and were kept constant during the first step of the molecular structure refinement discussed in the following section. Cell parameters of all polymers are given in Table 2.

Under the hypothesis that only one chain per unit cell is independent, we started the analysis by considering the centrosymmetric space group $P\bar{1}$. To build a reliable molecular model of **P**(2,3), one should take into account the constitutional disorder due to the statistical insertion of the *n*-propyloxy terephthalate unit along the macromolecular backbone. This was tentatively accounted for by generating two *n*-propyloxy groups, each the mirror image of the other taken with respect to a mirror plane perpendicular to the line connecting atoms C13 and C16 of the aromatic ring of the terephthaloyl group (Figure 10). An occupancy factor of 0.5 is imposed

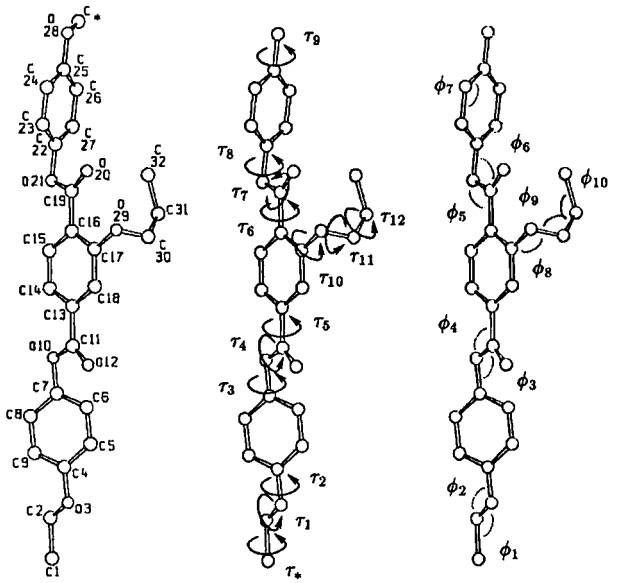

Figure 10. Bond and torsion angles setting chain structure. For the sake of clarity only one propyloxy group of the statistical model is shown.

on the atoms of both *n*-propyloxy groups. Successive trials to allow for a possible conformational disorder by an additional mirroring with respect to a plane lying on the aromatic ring of the terephthaloyl group led to unsatisfactory results.

The structural parameters setting the chain structure (bond lengths, torsion and bond angles) are defined in Figure 10 and Table 3. To ensure the convergence of the refinement procedure, the number of parameters should be reduced as much as possible. Usually, bond lengths and most bond angles are fixed at the standard values (see Table 3). On the contrary, torsion angles are expected to vary in a large range; thus, they have to be refined. The independent unit is free to rotate around the *c* axis and to move in the unit cell; thus, four more overall parameters have to be considered: the rotation angle Φ_o and the fractional coordinates x_o, y_o, and z_o. Φ_o is defined as the intersection angle between the $x-z$ plane and the plane containing the chain axis and atom C14. x_o, y_o, and z_o are the fractional coordinates of the geometrical center of the terephthaloyl aromatic ring.

In order to have a reasonable starting model for performing structure refinement and to ensure the convergence of the iterative process, the usual *trial* and *error* procedure was applied. In this stage, the terephthalate unit was set planar (τ_5 = 0°, τ_6 = 0°) and torsion angles τ_3 and τ_8 between the hydroquinone and the terephthaloyl moieties were fixed at 60°. The constraints $\phi_3 = \phi_6$, $\phi_4 = \phi_5$, and $\tau_4 = \tau_7$ were also imposed. The *n*-propyloxy unit was taken in the most extended conformation (τ_{10} = 0°, $\tau_{11} = \tau_{12}$ = 180°). $\vec{\rho}_t$ was placed coincident with *a** during the initial analysis (ω_t = 0, σ_t = 90°). Most of the information about the molecular structure could be deduced from the intensi-

Table 3

Structural Parameters Kept Fixed during the Refinement

Bond Lengths (Å)

l_1 (C−H)	1.08	l_2 (C−C)	1.54
l_3 (C−CO)	1.50	l_4 (C=O)	1.24
l_5 (O−C)	1.36	l_6 (C=C (phenylene ring))	1.40

Bond Angles (deg)

ϕ_1	109.5	ϕ_2	109.5
ϕ_7[a]	120	ϕ_8	109.5
ϕ_9	109.5	ϕ_{10}	109.5

Torsion Angles (deg) (for Atom Labeling See Figure 10)

τ_1	C1−C2−O3−C4	τ_2	C2−O3−C4−C5	τ_3	C6−C7−O10−C11
τ_4	C7−O10−C11−C13	τ_5	O10−C11−C13−C14	τ_6	C15−C16−C19−O21
τ_7	C16−C19−O21−C22	τ_8	C19−O21−C22−C23	τ_9	C24−C25−O28−C*
τ_{10}	C18−C17−O29−C30	τ_{11}	C17−O29−C30−C31	τ_{12}	O29−C30−C31−C32

[a] All the aromatic bond angles are kept fixed at 120° according to the canonical sp^2 geometry.

Table 4. Structural and Nonstructural Parameters As Obtained after Refining the Molecular Structure[a] (Torsion and Bond Angles Given in deg)

ϕ_3[b]	103.4(4)	ϕ_4[c]	107.8(4)				
τ_1	175.2(3)	τ_2	148(2)	τ_3[d]	30	τ_4	183.9(4)
τ_5	−10.7(6)	τ_6[d]	10	τ_7	173.9(3)	τ_8	69.1(7)
τ_9	167(1)	τ_{10}	−60.6(8)	τ_{11}	−81(1)	τ_{12}	−46(2)
τ^*	−54.9						
x_o	0.287(1)	y_o	0.267(1)	z_o	0.1525(8)		
Φ_o	−24.8(3)°						
Δa	107(1) Å	Δb	137(1) Å	Δc	357(28) Å	α_o	5.21(1)
a	13.20(1) Å	b	6.48(1) Å	c	20.11(2) Å		
α	138.3(1)°	β	110.9(1)°	γ	80.8(1)°		
V	1053 Å^3	d	1.367 g cm^{-3}				
μ	3.25(1)°	ω_t	−12.0(6)°				
B_{iso}	0.300						
R_1[e]	0.037	R_2[e]	0.040				

[a] Hydrogen atoms were included in the calculation by evaluating atomic coordinates according to sp^2 and sp^3 geometry. [b] $\phi_3 = \phi_6$. [c] $\phi_4 = \phi_5$. [d] Constrained condition. [e] R is the discrepancy index $\sum_i |I_{i,obsd} - I_{i,calcd}|^2 / \sum_i I_{i,obsd}$. $I_{i,obsd}$ and $I_{i,calcd}$ are respectively the observed and the calculated diffraction intensities at the generic ith point. R_1 and R_2 correspond to film no. 1 and film no. 2 with exposition times of 10 and 60 min, respectively.

ties of reflections 100, 200, 300, and 010. A strong 200 and a weak 100 spot suggest that the molecule is placed in a such a way that the fractional coordinates x of atoms are sharply distributed around $\bar{x} = 0.25$. Thus, applying the trial and error procedure, we found a rough agreement between calculated and observed patterns with the following values: $\tau_1 = 180°$, $\tau_2 = 160°$, $\tau_4 = 180°$, $\tau_9 = 120°$, $x_o = 0.24$, $y_o = 0.20$, $z_o = 0.10$, and $\Phi_o = -10°$.

Structure Refinement. Applying the whole-pattern procedure,[13] the structure refinement was carried out in four steps.

(1) The structural parameters were fixed to the values given in Table 3 and to those obtained in the preliminary *trial* and *error* stage. Cell parameters were fixed to the values given in the previous section. Then the nonstructural parameters, defining the background and the profile function, were refined. These are the average crystallite sizes, Δa, Δb, and Δc, the average angle of crystallites orientation, α_o, and the tilting angle, μ. Δa, Δb, and Δc are the crystallite sizes along directions parallel to the cell axes a, b, and c respectively. ω_t was refined in order to find the best direction of the tilting vector $\vec{\rho}_t$ which was taken coincident with a^* ($\omega_t = 0°$) in the initial analysis. σ_t was fixed at 90° during refinement, being strongly correlated to ω_t.

(2) All torsion angles, bond angles ϕ_3 (=ϕ_6), ϕ_4 (=ϕ_5), fractional coordinates x_o, y_o, z_o, and Φ_o were refined together while the nonstructural parameters were kept fixed at the values obtained in the previous step. The isotropic thermal parameter B_{iso}, set equal for all atoms, was not refined, being strongly correlated to the scale factor.

(3) Three constraints (Lagrange multipliers) were imposed during the refinement: (*i*) cell axis c must match the repetition unit length (chain continuity condition); (*ii*) bond angle C25−O28−C* (see Figure 10) is set equal to ϕ_2; (*iii*) torsion angles τ_3 and τ_6, when refined, are brought to unreliable values, with strong steric intramolecular interactions. The constrained conditions $\tau_3 = 30°$ and $\tau_6 = 10°$ ensure the convergence of the refinement. In terms of intramolecular conformational energy, these values are only slightly less favorable than the minimum energy ones.[14] Nonetheless, trials utilizing the latter values were performed. However, they led to a large fluctuation of the refined parameters.

(4) In the final run, all parameters were refined together.

The comparison between observed and calculated patterns is given in Figure 11. Refined parameters and atomic coordinates are listed in Table 4 and Table 5, respectively. Molecular packing is shown in Figures 12 and 13.

Intra- and intermolecular atomic distances are in agreement with the standard values [shortest values are the intermolecular C6−O18 (3.23 Å) and C5−C18 (3.25 Å) distances, between chains translated along the b axis direction], excepting those involving the *n*-propyloxy units (shortest contact is 3.01 Å for the O28−C30 intermolecular distance). Actually, the latter interactions have little physical meaning because of the

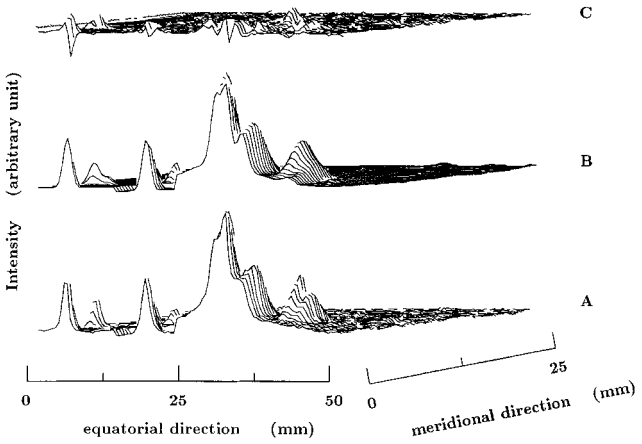

Figure 11. Three-dimensional representation of observed (A) and calculated (B) diffraction patterns, with the relative difference (C).

Table 5. Fractional Atomic Coordinates of P(2,3), Phase I

atom	x(σ_x)	y(σ_y)	z(σ_z)
C1	0.1767(61)	0.5878(60)	−0.3368(34)
C2	0.1636(63)	0.5763(58)	−0.2664(29)
O3	0.2570(31)	0.5085(71)	−0.2327(36)
C4	0.2422(31)	0.4727(58)	−0.1780(29)
C5	0.3311(21)	0.5581(58)	−0.0934(33)
C6	0.3159(16)	0.5213(41)	−0.0371(25)
C7	0.2116(35)	0.3991(54)	−0.0655(20)
C8	0.1228(68)	0.3138(92)	−0.1501(28)
C9	0.1382(64)	0.3508(84)	−0.2063(28)
C10	0.1968(40)	0.3633(66)	−0.0108(21)
C11	0.2965(8)	0.3090(30)	0.0209(16)
O12	0.3766(37)	0.2823(51)	−0.0022(27)
C13	0.2914(6)	0.2876(18)	0.0890(10)
C14	0.1906(39)	0.2744(49)	0.0950(17)
C15	0.1859(41)	0.2544(44)	0.1586(18)
C16	0.2820(6)	0.2476(18)	0.2160(10)
C17	0.3827(39)	0.2608(49)	0.2098(17)
C18	0.3873(41)	0.2808(44)	0.1463(18)
C19	0.2769(8)	0.2262(30)	0.2841(16)
O20	0.3521(31)	0.1775(62)	0.3274(21)
O21	0.1747(46)	0.2700(46)	0.2895(27)
C22	0.1819(44)	0.2806(40)	0.3612(30)
C23	0.1907(43)	0.0074(42)	0.3334(32)
C24	0.1981(46)	0.0184(53)	0.4072(38)
C25	0.1967(46)	0.3025(54)	0.5088(39)
C26	0.1880(53)	0.5754(47)	0.5364(37)
C27	0.1805(54)	0.5641(44)	0.4625(34)
O28	0.2039(49)	0.3131(69)	0.5805(44)
O29	0.4761(77)	0.2542(95)	0.2656(30)
C30	0.5480(99)	0.5266(120)	0.3377(36)
C31	0.5147(85)	0.7899(105)	0.4365(26)
C32	0.5003(106)	0.6768(152)	0.4786(45)

statistical model employed in the analysis. In fact, the method applied does not afford a description of the overall structure as a statistical average of several (local) structures, each being entirely stereochemically consistent.

Conclusion

The tilting of crystallites in fiber samples has been frequently observed in the case of polyesters.[15] In some cases, this effect has been ascribed to the structure of the macromolecular backbone. For instance, rigid and flexible moieties alternating along the chain may promote it,[16] probably because of the tendency of rigid moiety to orient along the direction of elongation. In the case of **P**(2,*n*), the tilting of crystallites increases by increasing *n* (see Table 2); thus, the length of *n*-alkoxy group plays a relevant role. At this stage of

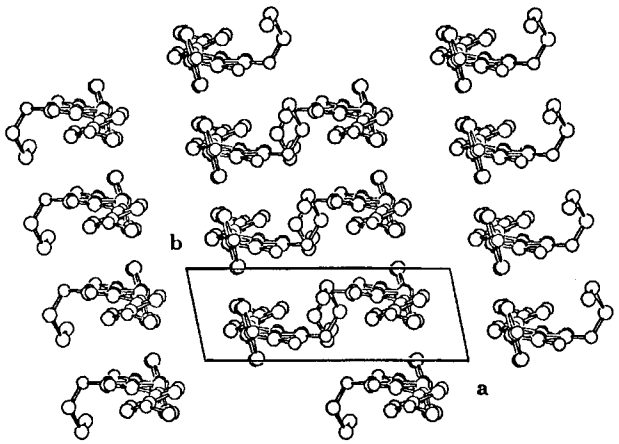

Figure 12. Molecular packing of **P**(2,3), phase I. A view of molecular packing along the *c* axis.

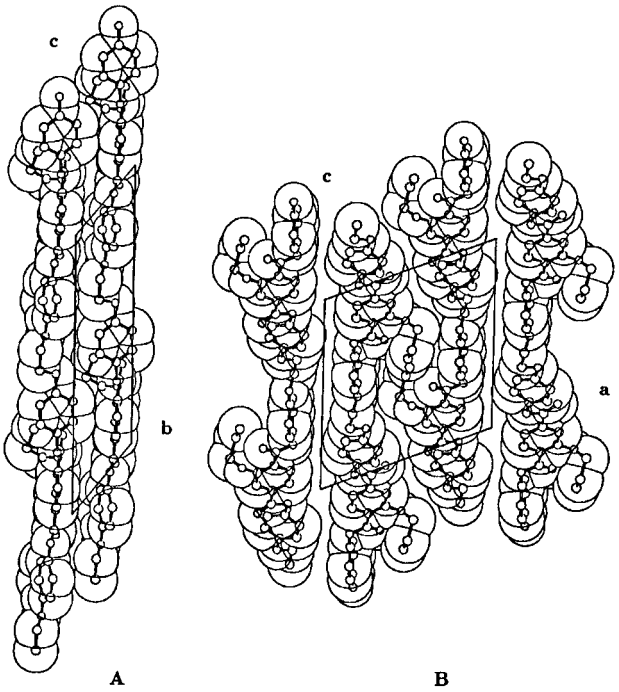

Figure 13. Molecular packing of **P**(2,3), phase I. Views of the molecular packing (A) along *a* and (B) along *b* axes, respectively.

investigation, we are not able to explain the reason for this effect.

Because of the center of symmetry, the backbones of the two chains in the unit cell of **P**(2,3) are in contact, while the *n*-propyloxy groups are placed at the opposite side. The repetition of the unit cell content by translation along the *b* axis direction leads to the packing of macromolecules in *double stacks*. This resembles very much that suggested by Stern *et al.* for the structure of poly(3−*n*-alkyl-4-oxybenzoate)s[2] and by Kricheldorf *et al.* for the structure of new sets of polyanhydrides[5,6] and poly(phenyleneterephthalimide)s[9] derived from monoalkyl thioterephthalate. The latter Authors suggest that a *back-to-back* arrangement of polymeric chains takes place due to the monosubstitution at the side chain. Blackwell *et al.* reported the interleaving of the side pendant along the *c* axis direction for the poly(phenyl-*p*-phenyleneterephthalate)[17] and its related copolymers,[18] but chains are organized to give a *single-stack* array.

Phase I is different from the crystalline phase reported for **P**(2,*n*) with $n > 4$.[10] In fact, the diffraction

patterns characterizing those polymers suggest a triclinic unit cell (seemingly with no correlation to the triclinic cell parameters of phase I) with larger *a* and *b* parameters and, consequently, with a higher number of chains per unit cell. On a purely hypothetical ground, this might be caused by some degree of *packing incompatibility* between lateral groups and backbone chains. This *incompatibility* would increase with the length of the *n*-alkoxy group promoting the organization of chain backbones in *bundles* with the confinement of the lateral substituents. This bundle would assume the shape of an almost perfect cylinder for **P**(2,8), according to the quasi-hexagonal cell observed[10] ($a = b = 21.22$ Å, $c = 20.86$ Å) with 12 chains accommodated in the unit cell.

Acknowledgment. Financial support by Ministero dell'Universitá e della Ricerca Scientifica e Tecnologica (MURST) and by Consiglio Nazionale delle Ricerche (CNR) is acknowledged.

References and Notes

(1) Ebert, M.; Herrmann-Schonherr, O.; Wendorff, J. H.; Ringsdorf, H.; Tschirner, P. *Liq. Cryst.* **1990**, *7*, 63.
(2) Stern, R.; Ballauff, M.; Lieser, G.; Wegner, G. *Polymer* **1991**, *32*, 2096.
(3) Watanabe, J.; Harkness, B. R.; Sone, M.; Ichimura, H. *Macromolecules* **1994**, *27*, 507.
(4) Sone, M.; Harkness, B. R.; Kurosu, H.; Ando, I.; Watanabe, J. *Macromolecules* **1994**, *27*, 2769.
(5) Kricheldorf, H. R.; Domschke, A. *Macromol. Chem. Phys.* **1994**, *195*, 943.
(6) Kricheldorf, H. R.; Domschke, A. *Macromol. Chem. Phys.* **1994**, *195*, 957.
(7) Watanabe, J.; Ono, H.; Uematsu, I.; Abe, A. *Macromolecules* **1985**, *18*, 2141.
(8) Galda, P.; Kistner, D.; Martin, A.; Ballauff, M. *Macromolecules* **1993**, *26*, 1595).
(9) Kricheldorf, H. R.; Domschke, A. *Macromolecules* **1994**, *27*, 1509.
(10) Caruso, U.; Iannelli, P.; Pragliola, S.; Roviello, A.; Sirigu, A. *Macromolecules* **1995**, *28*, 6089.
(11) Iannelli, P. *J. Appl. Crystallogr.* **1996**, *29*, 491.
(12) Immirzi, A.; Iannelli, P. *Macromolecules* **1988**, *21*, 768.
(13) Iannelli, P. *J. Appl. Crystallogr.* **1994**, *27*, 1055.
(14) Hummel, J. P.; Flory, P. J. *Macromolecules* **1980**, *13*, 479.
(15) Hall, I. H. In *Structure of Crystalline Polymers*; Hall, I. H., Ed.; Elsevier: London, 1984, and references therein.
(16) Carotenuto, M.; Guadagno, L.; Iannelli, P.; Chiellini, E.; Farah, A. A.; Galli, G. *J. Polym. Sci., Polym. Phys.* **1995**, *33*, 1097.
(17) Hong, S. K.; Blackwell, J. *Polymer* **1989**, *30*, 225.
(18) Hong, S. K.; Blackwell, J. *Polymer* **1989**, *30*, 780.

MA961523N